Electronic Supplementary Material (ESI) for Environmental Science: Atmospheres.

Supplementary material

Maria Paula Pérez-Peña,[*a] Jenny A. Fisher,[b‡] Christopher Hansen,[a] and Scott H. Kable[a]

September 27, 2023

CF_3CHO absorption cross section

Figure 1 shows the CF_3CHO absorption cross sections from 200-400 nm at 298 K reported by Sellevag *et al.* Sellevag et al., 2004.

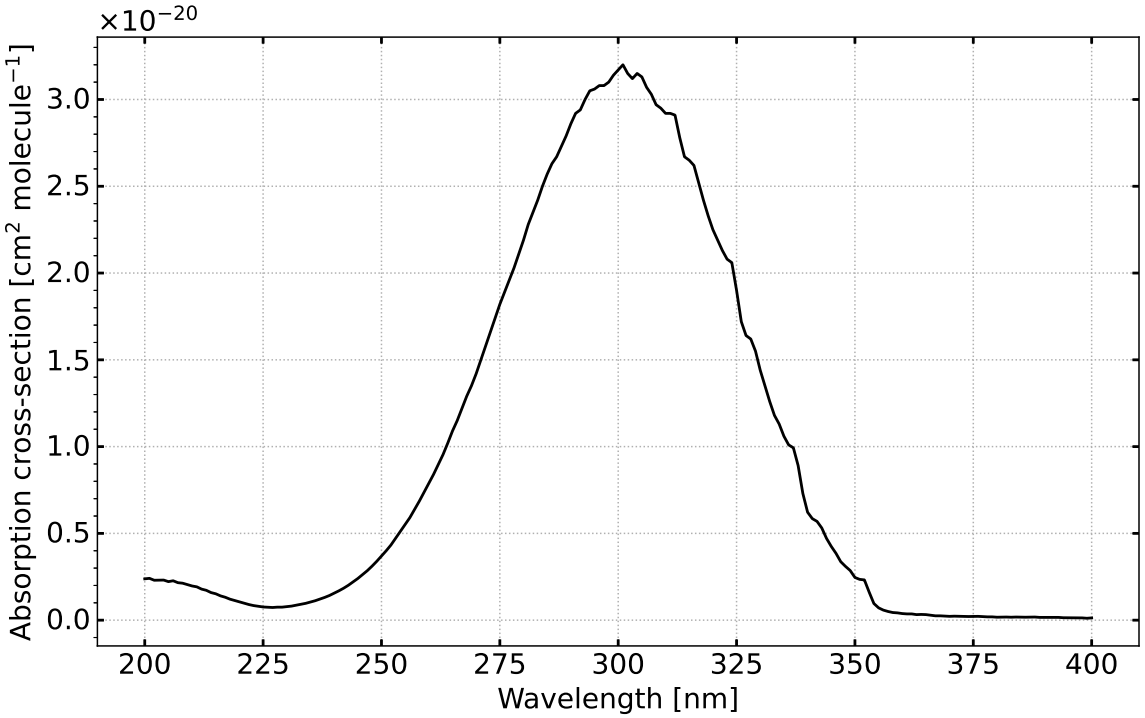

Figure 1: Absorption cross-section for CF_3CHO at 298 K as a function of wavelength, as reported by Sellevag et al. (2004).

Henry's Law parameters

Table 1 shows Henry's Law parameters for a series of simple oxygenated organic compounds. Acids and other species that are ionised in solution are excluded. Also recorded are the same compounds with a degree of fluorine substitution, especially substitution of a methyl group (CH_3) with a trifluoromethyl group (CF_3). In every case, replacing a CH_3 group with CF_3 reduces H^{cp} by about one to two orders of magnitude, *i.e.* increasing fluorination decreases solubility. In this work, we bracket $H^{cp}(CF_3CHO)$ by the values for CH_3CHO and CF_3CFO.

Table 1: Table of Henry's law solubility constant (H^{cp}), and the temperature dependence of H^{cp} ($\frac{dlnH^{cp}}{d(1/T)}$) for some oxgenated organic species and their fluorine substituted counterparts. Values obtained from Sander (2015) unless specified otherwise.

Compound	**Name**	H^{cp} [mol m^{-3} Pa^{-1}]	H^{cp} [M atm^{-1}]	$\frac{d(\mathbf{ln}H^{\mathbf{cp}})}{d(1/T)}$ [K]
HCHO	methanal (formaldehyde)	32.0	3240	7100
FCHO	formyl fluoride	0.030	3.0	-[b]
FCFO	carbonyl fluoride	$0.01 - 0.35$	$1 - 36$	-[b]
CH_3CHO	**ethanal (acetaldehyde)**	0.13	13.2	5900
CF_3CHO	**trifluoroethanal**	-[b]	-[b]	-[b]
CF_3CFO	**trifluoroacetyl fluoride**	$0.0095 - 0.03$	$0.96 - 3$[a]	-[b]
CH_3COCH_3	propanone (acetone)	27	2736	5500
CF_3COCH_3	1,1,1-trifluoro-2-propanone	1.4	142	8900
CH_3CH_2OH	ethanol	1.9	193	6400
CF_3CH_2OH	2,2,2-trifluoroethanol	0.47	47.6	6200
$CH_3CHOHCH_3$	2-propanol (isopropanol)	1.30	132	7500
$CF_3CHOHCH_3$	1,1,1-trifluoro-2-propanol	0.45	45.6	6300
$CF_3CHOHCF_3$	1,1,1,3,3,3-hexafluoro-2-propanol	0.24	24	6700
$CH_3CH_2OCH_2CH_3$	diethyl ether	0.011	1.1	$3900 - 6600$
$CH_3CH_2OCH_2CF_3$	ethyl 2,2,2-trifluoroethyl ether	0.00072	0.073	-[b]
$CH_3CH_2O(C{=}O)H$	ethyl methanoate (ethyl formate)	0.034	3.5	4600
$CF_3CH_2O(C{=}O)H$	2,2,2-trifluoroethyl methanoate	0.0054	0.55	4700

[a] Obtained from Burkholder et al. (2015)
[b] Not measured
[c] Obtained from Kim et al. (2023)

Acetaldehyde deposition

Figure 2 shows the resulting temporally averaged dry deposition velocities obtained for acetaldehyde. The highest global dry deposition velocity value modelled for acetaldehyde was 0.7 cm s^{-1} for both modelling periods. As expected, there was a marked seasonality in the estimates, mostly driven by the presence of snow in the Northern Hemisphere winter. For January, the acetaldehyde dry deposition velocities in the Northern Hemisphere did not exceed 0.23 cm s^{-1}, and the maximum dry deposition value was found to occur in equatorial regions. On the other hand, for June, the maximum dry deposition velocities of 0.7 cm s^{-1} were observed at higher Northern Hemisphere latitudes as well as in equatorial regions.

The acetaldehyde dry deposition velocities from GEOS-Chem are lower at tropical and equatorial regions than the observed and modelled values reported by Müller et al. (2019). Müller et al. (2019) report dry deposition velocities for two dominant plant functional types, tropical rainforest and pine plantation, ranging between 1.0 cm s^{-1} and 2.3 cm s^{-1}. On the other hand, our predictions are comparable to the modelled acetaldehyde dry deposition values over North America reported by Zhang et al. (2023). Averaged across two modelled years, the mean acetaldehyde dry deposition value for North America determined by Zhang et al. (2023) was 0.065 cm s^{-1}, while the maximum reported value was 0.56 cm s^{-1}. In Figure 2b, it can be observed that for June, our modelled dry deposition ranged from ∼0.2 cm s^{-1} to ∼0.6 cm s^{-1} over North America. We considered our acetaldehyde dry deposition velocities to be reasonable and thus suitable to be used as a reference for CF_3CHO.

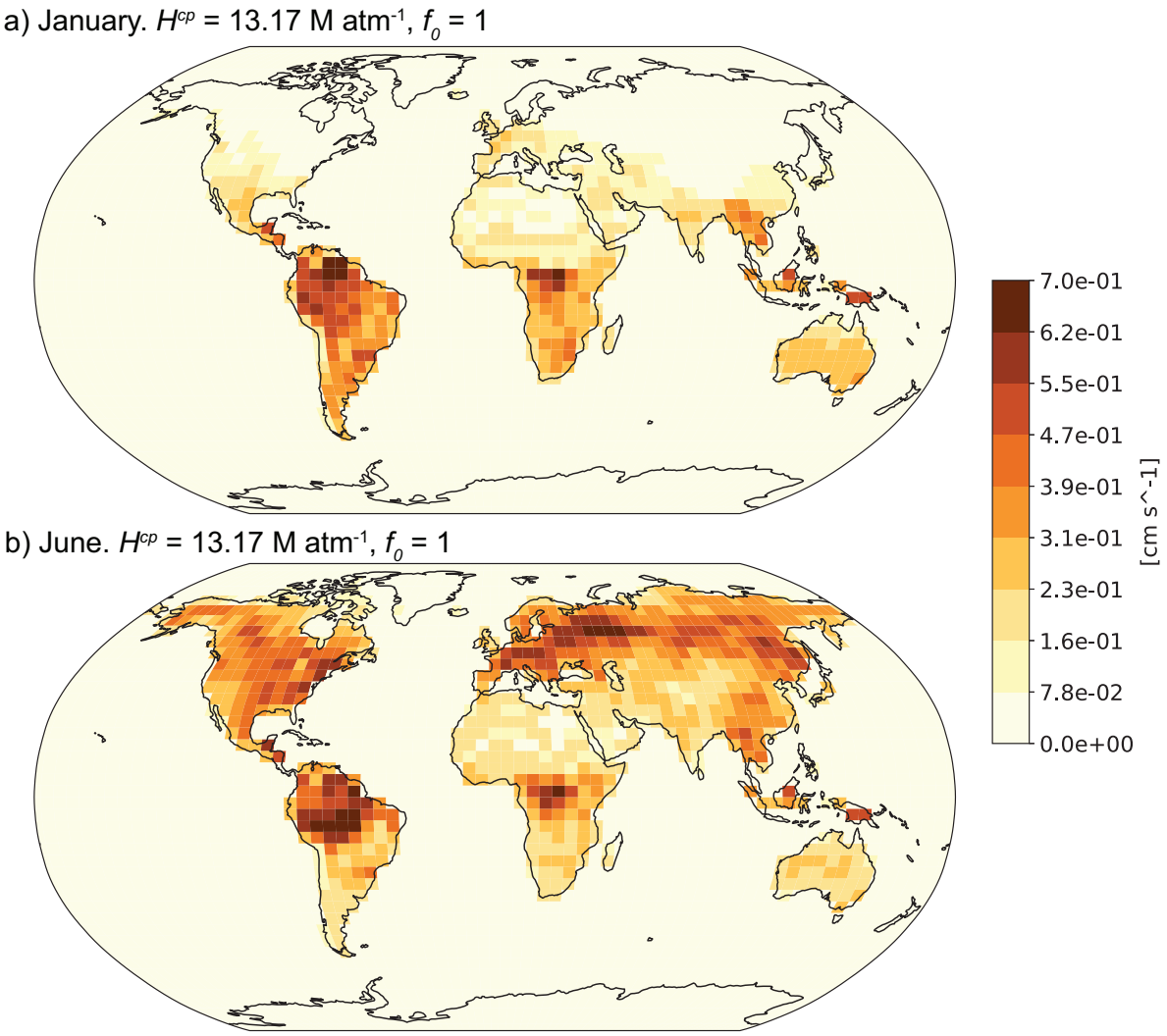

Figure 2: Average monthly dry deposition velocities for acetaldehyde modelled with GEOS-Chem for a) January b) June 2014

Modelled CF_3CHO deposition velocities for January 2014

Figure 3 complements the figure on dry deposition velocities for CF_3CHO in June 2014 shown in the main text (Figure 3).

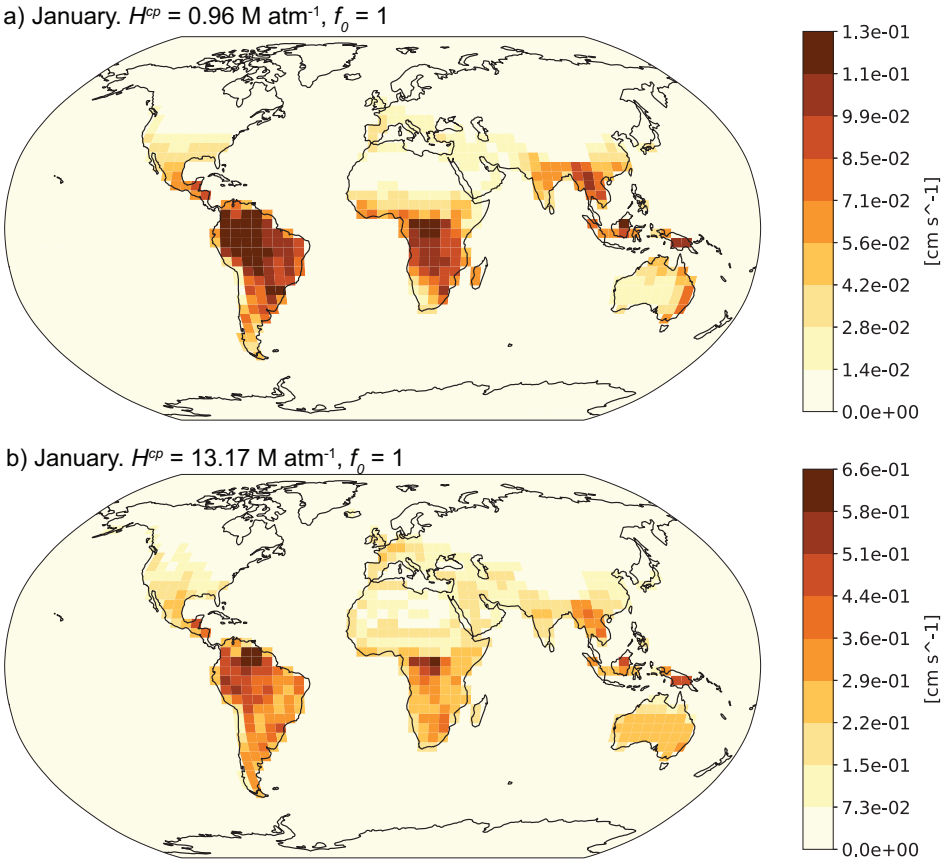

Figure 3: Average monthly dry deposition velocities determined using GEOS-Chem for CF_3CHO for January 2014 using H^{cp} of (a) 0.96 M atm^{-1} and $f_0 = 1$ and (b) 13.17 M atm^{-1} and $f_0 = 1$. The result of using $H^{\mathrm{cp}} = 0.96$ M atm^{-1} and $f_0 = 0$ were the same as when using $f_0 = 1$ (a) and are not shown here.

Modelled $OH^{\bullet}$

Figure 4 shows the daily average estimates of the $OH^{\bullet}$ concentration from the two atmospheric conditions tested in the box model. The urban site had higher concentrations of the $OH^{\bullet}$ radical compared to the pristine site. The daytime peak of $OH^{\bullet}$ in the pristine atmosphere of $\sim 4 \times 10^6$ molecules cm^{-3} was within the ranges modelled for $OH^{\bullet}$ by Whalley et al. (2010) of $(3.8-7.5) \times 10^6$ molecules cm^{-3} in this location. For the urban atmosphere, the peak concentration of $OH^{\bullet}$ was $\sim 5 \times 10^6$ molecules cm^{-3}, within the modelled $OH^{\bullet}$ reported by Whalley et al. (2018) at London of $(4-8) \times 10^6$ molecules cm^{-3}. The modelled urban $OH^{\bullet}$ peak is also broader in time than pristine atmosphere. Because the urban modelled atmosphere is located at a higher latitude than for the pristine atmosphere, the broader $OH^{\bullet}$ peak reflects a longer daylight period. These two features of the urban site, i.e., a higher and broader $OH^{\bullet}$ peak, result in faster consumption of HFO-1234ze and also CF_3CHO in the urban atmosphere.

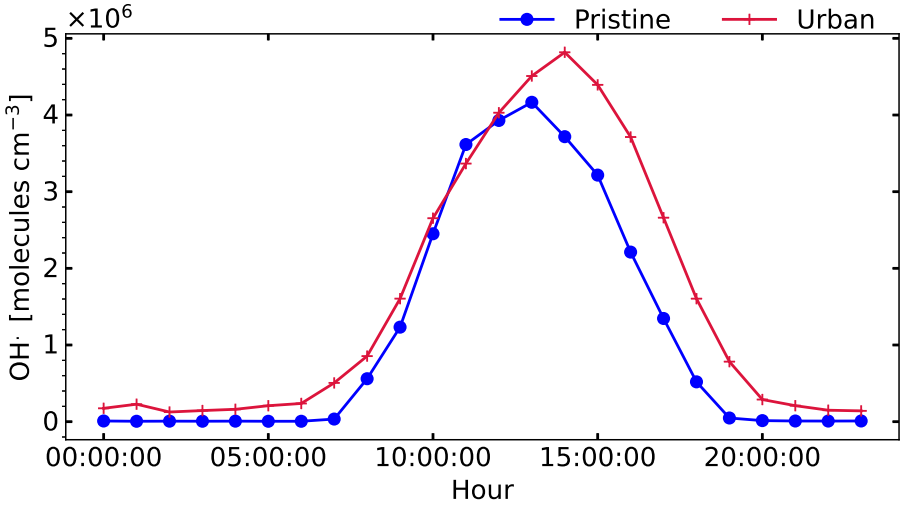

Figure 4: Hourly average $OH^{\bullet}$ modelled concentration in AtChem2 for the urban (*GU15_uqy_ndep* scenario red line with crosses) and pristine (*GP15_uqy_ndep* scenario blue line with circles) atmospheres.

Diel variation in CF_3CHO sinks

The diel variation of the four modelling sinks of CF_3CHO, i.e. OH reaction, photolysis to produce radicals, photolysis to produce FCS-23 and deposition, is shown in Figure 5. Three modelling scenarios are represented.

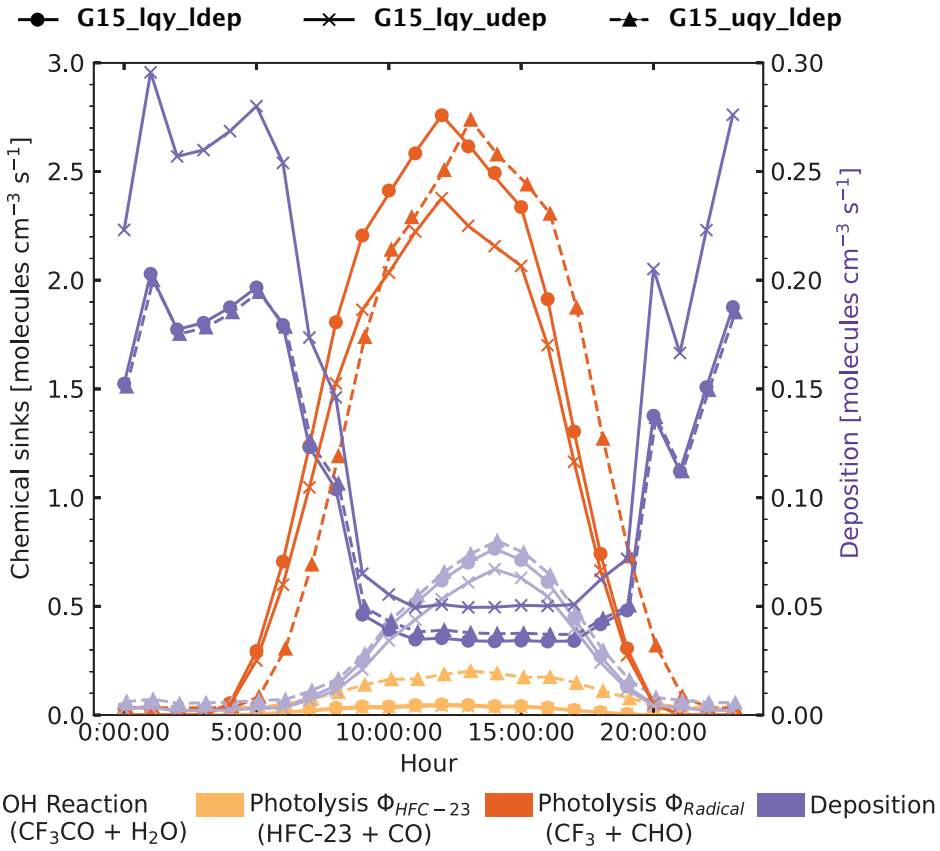

Figure 5: Average daily profile of the chemical and physical sinks of CF_3CHO in the atmosphere for three modelled scenarios: *G15_lqy_ldep* (continuous line with circles), *G15_uqy_ldep* (dashed line with triangles) and *G15_lqy_udep* (continuous line with crosses). For the latter, the deposition values are shown as $F_{dep}/10$.

References

Burkholder, J. B., Cox, R. A., & Ravishankara, A. R. (2015). Atmospheric degradation of ozone depleting substances, their substitutes, and related species. *Chemical Reviews*, *115*(10), 3704–3759. https://doi.org/10.1021/cr5006759

Kim, S., Chen, J., Cheng, T., Gindulyte, A., He, j., He, S., Li, Q., Shoemaker, B. A., Thiessen, P. A., Yu, B., Zaslavsky, L., Zhang, J., & Bolton, E. E. (2023). Pubchem 2023 update. compound summary. ethyl vinyl ether. *Nucleic Acids Research*, *51*(D1), D1373–D1380. https://doi.org/10.1093/nar/gkac956

Müller, J. F., Stavrakou, T., Compernolle, S., & Peeters, J. (2019). Chemistry and deposition in the model of atmospheric composition at global and regional scales using inversion techniques for trace gas emissions (magritte v1.1)-part 1: Chemical mechanism. *Geoscientific Model Development*, *12*(6), 2307–2356. https://doi.org/10.5194/gmd-12-2307-2019

Sander, R. (2015). Compilation of henry's law constants (version 4.0) for water as solvent. *Atmospheric Chemistry and Physics*, *15*(8), 4399–4981. https://doi.org/10.5194/acp-15-4399-2015

Sellevag, S. R., Kelly, T., Sidebottom, H., & Nielsen, C. J. (2004). A study of the ir and uv-vis absorption cross-sections, photolysis and oh-initiated oxidation of cf3cho and cf3ch2cho. *Physical Chemistry Chemical Physics*, *6*, 1243–1252. https://doi.org/10.1039/B315941H

Whalley, L. K., Furneaux, K. L., Goddard, A., Lee, J. D., Mahajan, A., Oetjen, H., Read, K. A., Kaaden, N., Carpenter, L. J., Lewis, A. C., C. Plane, J. M., Saltzman, E. S., Wiedensohler, A., & Heard, D. E. (2010). The chemistry of oh and ho2 radicals in the boundary layer over the tropical atlantic ocean. *Atmospheric Chemistry and Physics*, *10*(4), 1555–1576. https://doi.org/10.5194/acp-10-1555-2010

Whalley, L. K., Stone, D., Dunmore, R., Hamilton, J., Hopkins, J. R., Lee, J. D., Lewis, A. C., Williams, P., Kleffmann, J., Laufs, S., Woodward-Massey, R., & Heard, D. E. (2018). Understanding in situ ozone production in the summertime through radical observations and modelling studies during the clean air for london project (clearflo). *Atmospheric Chemistry and Physics*, *18*, 2547–2571. https://doi.org/10.5194/acp-18-2547-2018

Zhang, L., He, Z., Wu, Z., Macdonald, A. M., Brook, J. R., & Kharol, S. (2023). A database of modeled gridded dry deposition velocities for 45 gaseous species and three particle size ranges across north america. *Journal of Environmental Sciences (China)*, *127*, 264–272. https://doi.org/10.1016/j.jes.2022.05.030